Sea Surface Reflection Coefficient Estimation

Okwudili C. Orji PGS, Walter Sollner PGS, and Leiv J. Gelius UiO*

Summary

Sea surface reflection coefficient estimates are obtained from imaged sea surfaces by applying an imaging technique that is based on decomposed wavefields acquired by dual-sensor towed streamers. The accuracy of this technique in the case of imaging has been demonstrated employing controlled data scattered by realistic time-varying rough sea surfaces (e.g., Pierson-Moskowiz sea surface). The scattered data was computed based on the Kirchhoff-Helmholtz integral. Here, the feasibility of recovering sea surface reflection coefficient estimates from deterministic and realistic sea surfaces is demonstrated. First, using existing studies, the sea surface reflectivity is benchmarked. Subsequently, sea surface imaging was employed to demonstrate the feasibility of recovering the sea surface reflectivity from marine seismic data.

Introduction

The sea surface reflection coefficient is a vital but neglected input parameter in various seismic data processing algorithms. Traditional flat and stationary sea surface assumptions allow distortions caused by time-varying rough sea surfaces to persist in the processed data. It is a well-known fact that the sea surface acts as a mirror during seismic data acquisition causing a phenomenon called ghosting (Ghosh, 2000). Marine seismic ghosts cause notches in the spectrum of the acquired data which compromises seismic resolution. The attenuated frequencies depend on the depth of the source and the receiver. In surface related multiple elimination, SRME (e.g., Berkhout and Verschuur, 1997) and related methods of surface multiple suppression, removing all sea surface effects is the main goal (e.g., Fokkema and van den Berg, 1993). However, sea surface influence in shape and reflection coefficient is commonly ignored.

Modern seismic acquisition technology is rapidly advancing and presently, pressure and particle velocity sensors are towed in the streamers in order to eliminate the receiver side ghost (Carlson et al., 2007; Tenghamn et al., 2007; Özdemir et al., 2010). However, particle velocity sensors are sensitive to vibration noise especially at low frequencies. A practical approach to mitigate this problem is to reconstruct these low frequencies from the data measured by the pressure sensor. This process, termed Low Frequency Compensation (LFC), involves deconvolving the hydrophone ghost from the pressure sensor measurement and convolving with the ghost from the velocity and finally scaling the result by the appropriate impedance (Day et al., 2013). A possible problem with this method is the assumption that the sea surface reflection coefficient is -1.

On the source side, the diversity of the notches (dictated by source depths) in the spectrum of the acquired data is exploited in eliminating the source-side ghost. Data acquired by dual sources towed at different depths such that the notches in their spectrum are complimentary can be deghosted (Ziolkowski, 1971; Posthumus, 1993; Parkes and Hegna, 2011). Nonetheless, sea surface reflectivity is assumed -1 in applying this method. While this may suffice for low frequencies, higher frequencies are sensitive to the sea surface shape.

The effects of rough sea surface on time-lapse seismic data have been demonstrated by Laws and Kragh (2002). Rough sea scattering has been extensively studied. Eckart (1953), Holford (1981) and Orji et al., (2012) among others computed the scattered wavefield from rough surfaces employing the Kirchhoff-Helmholtz integral. McCammon and McDaniel (1985) obtain the reflection coefficient for a sinusoidal surface using very high frequencies. To the knowledge of the authors no attempt has been made to estimate sea surface reflection coefficients from seismic wavefields scattered by the sea surface.

Theory

Sea surface images can be obtained from data acquired by dual sensor streamers. This is achieved by separating the wavefield into the upgoing and downgoing components then extrapolating them upwards to the sea surface where an adequate imaging condition is applied (Orji et al., 2010 and 2012). The method was validated by computing wavefields scattered by realistic rough sea conditions using the Kirchhoff-Helmholtz integral. In this paper, we present sea surface reflection coefficient estimates obtained by dividing scattered wavefield amplitude from a rough sea surface in the frequency-wavenumber domain by that reflected by the flat sea surface equivalent. As a quality control, we compute the reflection coefficient from a sinusoidal surface and compare it with existing studies from optics. Subsequently, we show that similar results can be obtained using seismic parameters.

Scattering of sound from a pressure release sinusoidal surface, $f(x) = h\cos((2\pi/\Lambda)x)$, results in coherent and incoherent scattered wavefields characterized by discrete reflection orders whose angles of reradiation obey the diffraction grating equation (see Fig 1):

Sea Surface Reflection Coefficient

$$\cos\varphi_n = \cos\varphi_0 + \left(\frac{n\lambda}{\Lambda}\right) \qquad 1$$

In Fig 1 and Eqn 1, h and Λ are respectively the amplitude and wavelength of the sinusoidal surface, φ_0 is the incident angle of a planewave of wavelength λ on the surface, R_0 is the specular reflection in the direction φ_0, R_n are non-specular reflection orders in the directions φ_n and $[x', f(x')]$ is the surface height at lateral position x'. Thus, for a wavefield with a given incident angle on a surface the scattered amplitudes in different directions can be recovered.

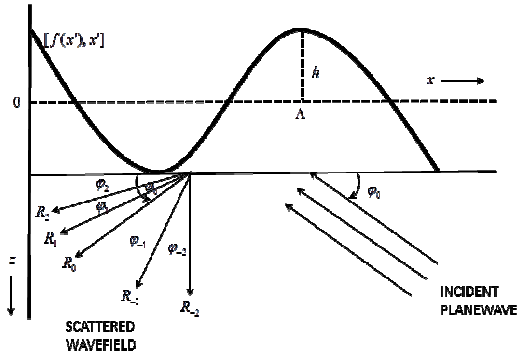

Figure 1: Geometry of scattering from a sinusoidal surface

In order to compute scattered wavefields from a surface we employ the Kirchhoff-Helmholtz integral (e.g. Holford 1981, Orji et al., 2012):

$$P(\bar{r},\omega) = e^{ik((z_0 - z_G)\cos\varphi_0 - (x_0 - x_G)\sin\varphi_0)} S(\omega) + \frac{1}{4i}\int_{\partial M}\left[H_0^{(1)}(k|\bar{r}' - \bar{r}|)\right]\frac{\partial P(\bar{r}',\omega)}{\partial n'}dl', \qquad 2$$

where $H_0^{(1)}$ is the zero-order Hankel function of the first kind, k is the wavenumber, ω is the frequency, ∂M is the length parameter along the sea surface, $\bar{r}'$ is a vector from the origin to $[x', f(x')]$, $\bar{r}$ is a vector from the origin to a receiver, $\bar{r}' - \bar{r}$ is a vector from $[x', f(x')]$ to a receiver at $G(x_G, z_G)$ with vertical and horizontal coordinates denoted as x_G and z_G respectively and n' is normal at x' on the surface (see Fig 2). $S(\omega)$ is the source pulse which can be set to 1 if only the Green's functions are needed. The first term in Eqn 2 is the incident planewave while the second term is the scattered wavefield. Eqn 2 is a Fredholm integral of the first kind and the unknown normal derivatives of the pressure field on the surface $\frac{\partial P(\bar{r}',\omega)}{\partial n'}$ can be obtained by numerical inversion, tagged HE, or by assuming that the radius of curvature of the sea surface is large compared with the wavelength of the wavefield (i.e., Kirchhoff approximation), tagged HK (see Orji et al., 2012).

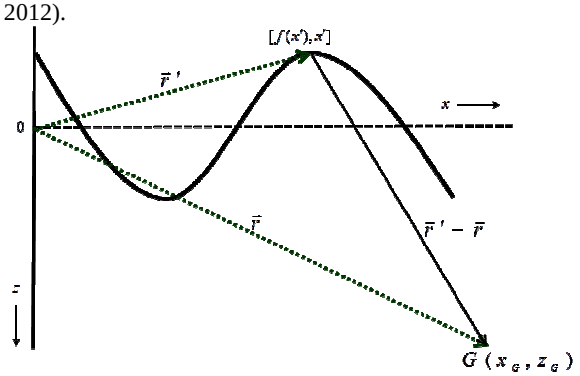

Figure 2: Sketch showing receiver position for computing scattered data.

Examples

Benchmarking

Data was generated for a sinusoidal surface of wavelength 50 m and wave height 2 m for 128 channels spaced at 6.25 m and placed at 50 m depth in a water medium. A planewave of wavelength approximately 16.7 m was incident on the surface at an incidence angle of 15°. Fig 3 shows the scattered wavefield in $\omega - k$ domain with various modes of the scattered wavefields indicated. The modes are in conformity with Fig. 1 and Eq. (1).

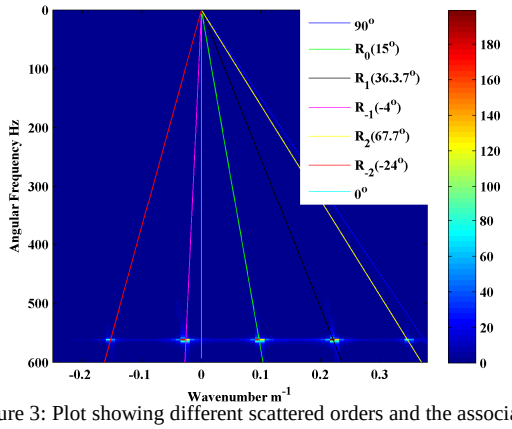

Figure 3: Plot showing different scattered orders and the associated directions using HK method.

Subsequently, specular reflection coefficient estimates for the sinusoidal surface (shown in the upper panel of Fig 4) are obtained by normalizing the scattered amplitude in the specular direction with the amplitudes from a flat surface. This example corresponds to an incidence angle of 40° and with wavelengths of the incident wavefield ranging from

approximately 0.0030 m - 1 m. This study is a reproduction of results obtained by McCammon and McDaniel (1985). In computing the data shown in Figs 3 and 4, HK is used.

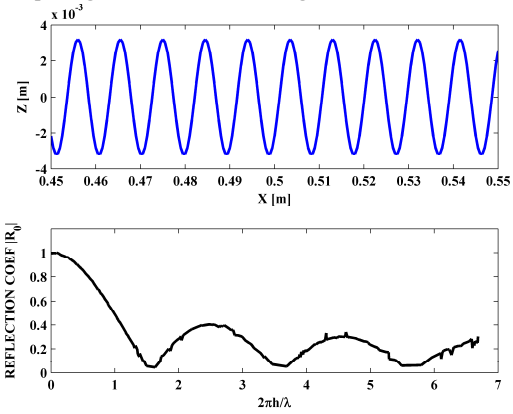

Figure 4: A sinusoidal surface (top) from which reflection coefficient in the specular direction (bottom) is computed using HK method.

Marine seismic case

We demonstrate that similar results can be obtained using seismic frequencies. This is achieved using the same approach as above by appropriately scaling the sinusoidal surface and the wavefield. Thus, scattered data is computed for 128 receivers spaced by 3m for 30° incident planewaves of frequencies ranging from 0-250 Hz. The surface is a sinusoid of amplitude 6m, wavelength 25m and discretized by 1m. Fig 5 shows the computed reflection coefficient in specular direction for the HE and HK algorithms. As expected and in accordance with results obtained by Eckart (1953) and later by McCammon and McDaniel (1985), HK failed to correctly predict unity when all side orders are evanescent (i.e., at 1st order cutoff region) and in addition show a shift in location of the reflection nulls.

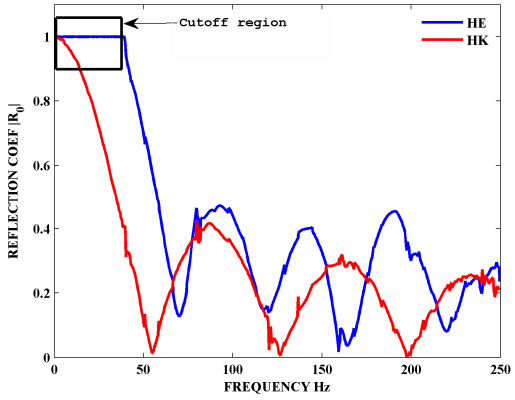

Figure 5: Specular reflection coefficients for data computed based on HE and HK for a sinusoidal surface.

Data was computed for a realistic sea condition using a similar set-up as above except that now the sea surface is computed from a Pierson-Moskowitz spectrum (PM) for 15 m/s wind speed (see Orji et al., 2012).. This rough sea surface condition (Fig 6 top panel) is chosen to demonstrate that HK and HE give similar results for a rough sea condition. This is because a rough surface is a superposition of many sinusoidal surfaces of different wavelengths. Thus, their reflection nulls occur at different frequencies. This diversity in null locations results in cancellation of these nulls leading to very similar results for HE and HK as shown in bottom panel of Fig 6.

We then use HK to compute reflection coefficient estimates for different incident angles (i.e., different receiver positions) since it is computationally faster. The incident angles covered are from 0° to 60° in intervals of 5° which is typical for marine seismic data. Fig 7 shows a surface plot of the reflection coefficients. Observe that for all angles and for frequencies between 0 and 15 Hz approximately, a flat and stationary sea surface assumption may suffice. However, the same assumption is erroneous for higher frequencies and especially smaller angles.

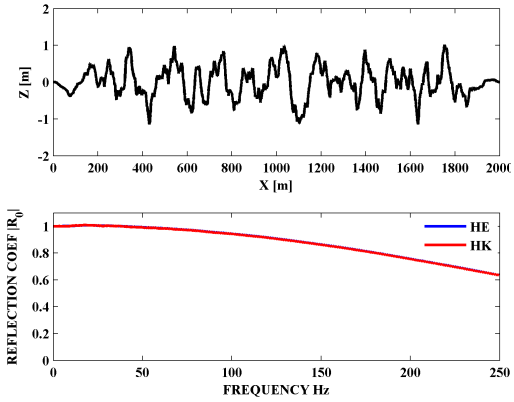

Figure 6: Pierson-Moskowitz sea surface for 15 m/s wind speed.

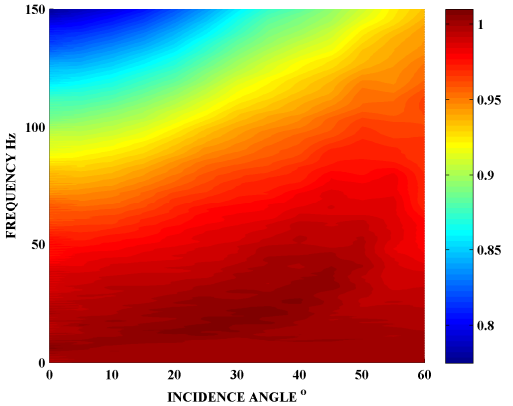

Figure 7: Reflection coefficients for different frequencies and incident angles computed from the rough sea surface in Fig 5.

Subsequently, we show that similar effects can be observed in field data. First using the field data acquired by PGS using dual-sensor streamer, we performed wavefield separation. Then we extrapolated the separated wavefields upwards to the sea surface where an imaging condition was applied in order to recover the sea surface variations (Orji et al., 2010 and 2012). Fig 8a shows the imaged sea surface which appears smoother in comparison to the PM sea surface. This is caused by the limited frequency band of the seismic source. However, it will be shown later, using the corresponding spectra of these sea surfaces, that they are in fact comparable.

Secondly, the sea surface imaged from field data is then employed in the HK algorithm. Here, we also considered incident angles of 0° to 60° but in intervals of 10°. Fig 8b shows a contour plot of the reflection coefficient for different frequencies and incidence angles, which shows a similar behavior as in the PM sea surface case. Fig 9 shows a direct comparison of the reflection coefficients for the PM sea surface and imaged sea surface from field data for two incidents angles (0° and 60°). We observe that sea surface roughness has more impact on the reflection coefficients at smaller incidence angles and relaxes as the incidence angle increases. Thus, the rougher the sea surface, the steeper the changes in reflection coefficient with decreasing incidence angle and vice versa (cf. Fig 9).

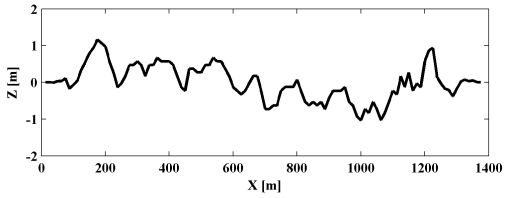

Figure 8a: Sea surface image from field data.

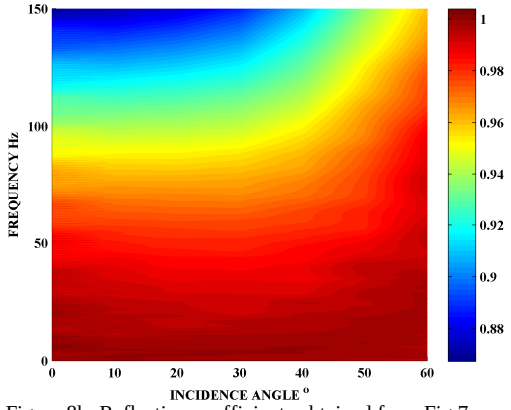

Figure 8b: Reflection coefficients obtained from Fig 7a.

The spectra of the sea surfaces shown in the lower panel of Fig 9 show that the simulated PM sea surface is very similar to the sea surface imaged from the field data. However, it can be observed that the sea surface from field data has been smoothed (the spectrum is shifted to lower wavenumbers). This is primarily due to the band limited source pulse used in acquiring the seismic data. Therefore, only this smoothed structure of the sea surface affects our seismic data. This is supported by the reflection coefficient trends in this paper: at very low frequencies (i.e., high wavelengths) of the seismic pulse, the sea surface variations are not seen. Nevertheless, in case of higher frequencies (if present in the acquired seismic data), the variations in reflection coefficient are underestimated.

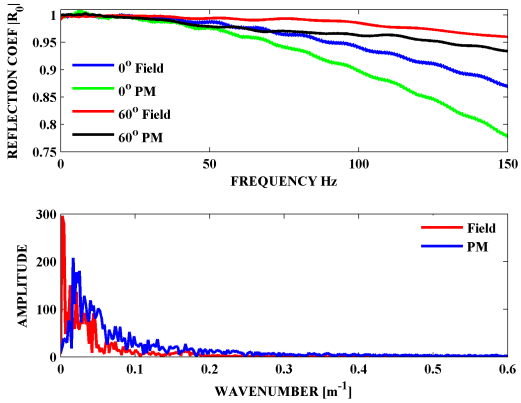

Figure 9: Comparison of reflection coefficients for PM and field data sea surfaces (top) and spectrum of the sea surfaces (bottom).

Conclusions

Estimation of reflections from imaged sea surfaces has been demonstrated and the reflection coefficient behaviors with frequencies and along the streamer have been investigated. We have validated this approach for different sea surface conditions using sinusoidal, synthesized realistic sea surfaces, and imaged sea surface from field data. Moreover, we show that the principal errors of HK are a shift in the location of the reflection nulls and inability to predict unity when all side orders are evanescent for sinusoidal surfaces. We show in addition that for rough sea surfaces these errors are negligible.

We have demonstrated that reflection coefficient changes with frequency and incidence angles. In addition, we show that the rougher the surface the sharper the changes especially for small incidence angles and high frequencies.

Acknowledgments

We thank PGS for permission to present this work. Orji wishes to thank his colleagues at PGS' G & E department for useful discussions.

http://dx.doi.org/10.1190/segam2013-0944.1

EDITED REFERENCES

Note: This reference list is a copy-edited version of the reference list submitted by the author. Reference lists for the 2013 SEG Technical Program Expanded Abstracts have been copy edited so that references provided with the online metadata for each paper will achieve a high degree of linking to cited sources that appear on the Web.

REFERENCES

Berkhout, A. J., and D. J. Verschuur, 1997, Estimation of multiple scattering by iterative inversion, Part I: Theoretical considerations: Geophysics, **62**, 1586–1595.

Carlson, D., A. Long, W. Söllner, H. Tabti, R. Tenghamn, and N. Lunde, 2007, Increased resolution and penetration from a towed dual-sensor streamer: First Break, **25**, 71–77.

Day, A., T. Klüver, W. Söllner, H. Tabti, and D. Carlson, 2013, Wavefield-separation methods for dual-sensor towed-streamer data: Geophysics, **78**, no. 2, WA55–WA70.

Eckart, C., 1953, The scattering of sound from the sea surface: Journal of the Acoustical Society of America, **25**, 566–570.

Fokkema, J. T., and P. M. van den Berg, 1993, Seismic applications of acoustic reciprocity: Elsevier Science Publ. Co.

Ghosh, S. K., 2000, Deconvolving the ghost effect of the water surface in marine seismics: Geophysics, **65**, 1831–1836.

Holford, R. L., 1981, Scattering of sound waves at a periodic, pressure-release surface: An exact solution: Journal of the Acoustical Society of America, **70**, 1116–1128.

Laws, R., and E. Kragh, 2002, Rough seas and time-lapse seismic: Geophysical Prospecting, **50**, no. 2, 195–208.

Orji, O., W. Söllner, and L. J. Gelius, 2010, Imaging the sea surface using a dual-sensor towed streamer: Geophysics, **75**, no. 6, V111–V118.

Orji, O., W. Söllner, and L. J. Gelius, 2012, Effects of time-varying sea surface in marine seismic data: Geophysics, **77**, no. 3, P33–P43.

Özdemir, K., A. Özbek, D.-J. van Manen, and M. Vassallo, 2010, On data-independent multicomponent interpolators and the use of priors for optimal reconstruction and 3D up/down separation of pressure wavefields: Geophysics, **75**, no. 6, WB39–WB51.

Parkes, G., and S. Hegna, 2011, Acquisition system that extracts the earth response from seismic data: First Break, **29**, no. 12, 81–87.

Pierson, W. J., and L. Moskowitz, 1964, A proposed spectral form for fully developed wind seas based on the similarity theory of S. A. Kitaigorodskii: Journal of Geophysical Research, **69**, 5181–5190.

Posthumus, B. J., 1993, Deghosting using a twin streamer configuration: Geophysical Prospecting, **41**, 267–286.

Tenghamn, R., S. Vaage, and C. Borresen, 2007, A dual-sensor towed marine streamer: Its viable implementation and initial results: 77th Annual International Meeting, SEG, Expanded Abstracts, 989–993.

Ziolkowski, A., 1971, Design of a marine seismic reflection profile system using air guns as a sound source: Geophysical Journal of the Royal Astronomical Society, **23**, 499–530.